THE JOURNAL OF PHYSICAL CHEMISTRY C

pubs.acs.org/JPCC Article

# First-Principles Study of Fluorinated Tetrahexcarbon: Stable Configurations, Thermal, Mechanical, and Electronic Properties

Mehmet Emin Kilic* and Kwang-Ryeol Lee*

Cite This: *J. Phys. Chem. C* 2020, 124, 8225−8235 Read Online

ACCESS | Metrics & More | Article Recommendations | Supporting Information

**ABSTRACT:** Tetrahexcarbon (TH-carbon) was recently predicted to be a stable two-dimensional semiconductor with an intrinsic direct band gap, making it promising for practical applications in optoelectronic devices. In this work, *ab initio* density functional theory (DFT) calculations were performed in order to study the possibility of manipulating the essential physical and chemical properties of TH-carbon by fluorination, which significantly change the hybridization states of carbon atoms. The phonon spectrum, *ab initio* molecular dynamics (AIMD) simulations, and elastic constants results revealed that fluorinated derivatives of TH-carbon are dynamically, thermally, and mechanically stable. Depending on the fluorine coverage, we examined the tunability of the electronic band gap and the direct−indirect−direct band gap transitions. We found that the phononic gap in TH-carbon can be controlled by fluorination. A decrease in the specific heat capacity was observed with increasing fluorine coverage, which is useful for nanoscale engineering of heat management. The fluorination is found to reduce the in-plane stiffness and Young's modulus but it increases the ultimate strength. These results suggest fluorination would enable the ability to tailor TH-carbon material for several interesting technological applications.

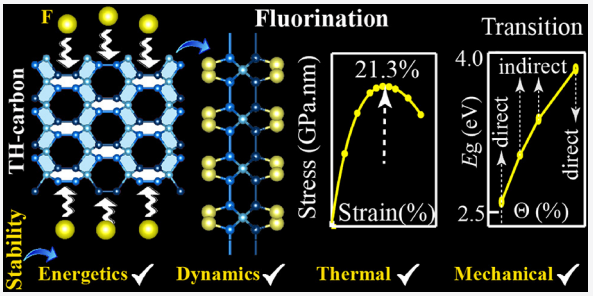


## INTRODUCTION

Two-dimensional (2D) materials (graphene,[1] silicine,[2] hexagonal boron nitride,[3] and many more[4−8]) have been the focus of a vast amount of attention. Graphene, as the most stable 2D form of carbon, has received a great deal of attention from experimentalists and theoreticans due to its superior properties such as the flexibility, zero gap, Dirac cone electronic structure, and high electron mobility.[1,9−11] The intense interest focused on graphene has motivated searches for the discovery of new carbon allotropes.

Carbon possess different hybridization states such as sp, $sp^2$, and $sp^3$ ones. Their combinations ($sp-sp^2$, $sp-sp^3$, and $sp^2-sp^3$) lead to form many possible atomic arrangements and reveal new carbon allotropes whose chemical and physical properties are quite different. For instance, $sp^3$-hybridization-diamond (3D structure) exhibits excellent hardness and insulating property whereas $sp^2$-hybridization-graphite layers (2D structure) are soft and zero band gap semiconductor.[1,12] Moreover, $sp-sp^2$ hybridization-6,6,12 graphyne has more amazing electronic and transport properties than that of graphene.[13] Furthermore, $sp^2-sp^3$-hybridization-pentagraphene (PG) possesses an unusual negative Poisson's ratio and ultrahigh ideal strength.[14] By applying a simple Stone−Wales transformation in PG, $sp^2-sp^3$-hybridized TH-carbon,[15] energetically more favorable than PG, has been recently predicted to be a stable two-dimensional-layered semiconductor with an intrinsic direct band gap and presents high electron mobility and highly anisotropic electronic properties. By designing the hybridization of carbon, we can change the essential phyical and chemical properties of these systems.[16]

Both experimental and theoretical efforts have revealed that chemical functionalizations of the carbon allotropes with adatom (H, F, O, and so forth) and ad-molecules (OH) can modify the hybridization of carbons. Hydrogenation[5,17] and halogenation (especially with fluorine atoms)[6,18,19] of graphene have been intensively investigated in recent years because of their many unique properties. For instance, hydrogenation in graphene transforms the hybridization of carbon from $sp^2$ to $sp^3$, changes its nature of electronic states from the semimetallic feature into a wide band gap semiconductor and induces magnetic moments and the extreme modification of the optoelectronic and transport properties.[5,20−24] Very recently, Kilic et. al reported the tunability of the phononic and electronic band gap and the direct−indirect−direct band gap transitions in TH-carbon by hydrogenation.[16] There is a significant chemical bonding interaction between halogen atoms and carbon atoms due to the strong electron affinities of halogen atoms, which play a critical role in geometric structures and electronic properties.

Received: December 30, 2019
Revised: March 18, 2020
Published: March 24, 2020

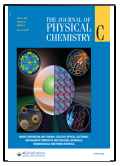







https://dx.doi.org/10.1021/acs.jpcc.9b12022
J. Phys. Chem. C 2020, 124, 8225−8235

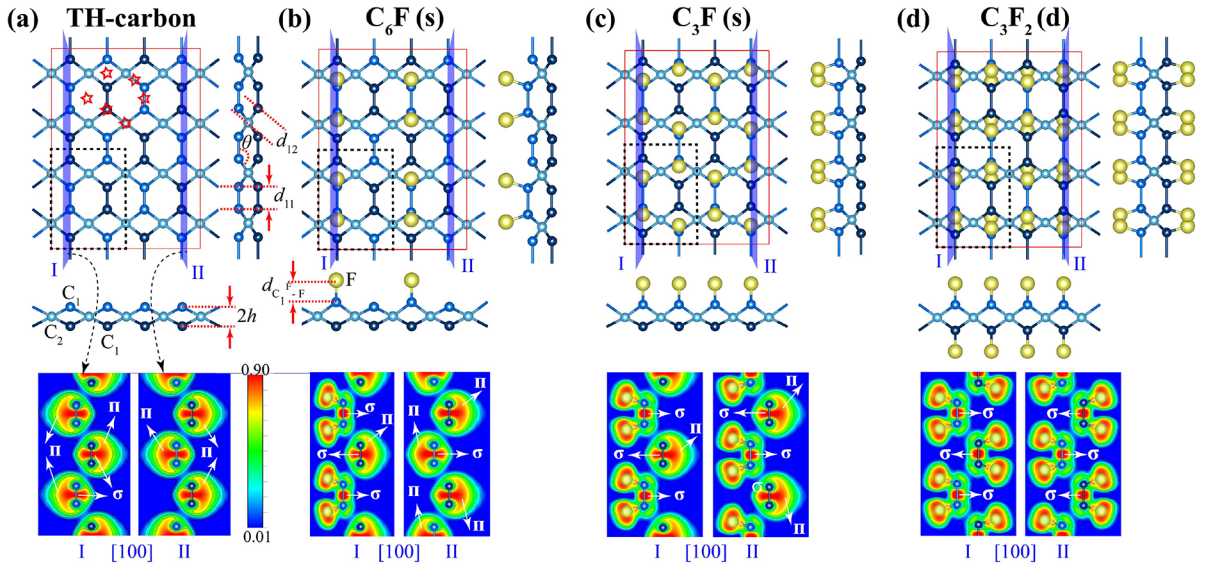


**Figure 1.** Top view along the [001] direction (upper panel left), side view along the [100] direction (upper panel right), another side view along the [010] direction (middle panel), and ELF profiles (lower panel) of (a) pristine TH-carbon, (b) $C_6F$(s), (c) $C_3F$(s), and (d) $C_3F_2$(d) in the 2 × 2 supercell framed by a rectangular red line. The unit cell of each considered system is also framed by a black dashed line. Here, the $sp^2$-hybridized carbon atoms ($C_1$) lie on two external layers while the $sp^3$-hybridized carbon atoms ($C_2$) lie on the middle layer. $C_1$ and $C_2$ atoms are blue and F is yellow. For each structure, two ELF profiles from the [100] planes are depicted, namely I and II. The ELF is dimensionless and has a range from 0 to 1. ELF = 1 means highly localized and bounded electrons, while ELF = 0 means lack of electrons.

Recently, fluorinated graphene has been reported to be more stable than hydrogenated graphene at higher temperatures.[25] Besides hydrogenation, fluorinated graphene exhibits many unique properties such as opened bandgap and high thermal and chemical stability because of the formation of various types of C—F bonds (covalent, semi-ionic, or ionic) resulting from the high difference in electronegativity between C (2.5) and F (4.0).[25,26] Recently, much progress has been made on the preparation and control of C—F bonding characters, F/C ratios (the F/C ratio is defined as the mole ratio of fluorine to carbon), and configurations of fluorinated graphene.[19,25]

In this present work, we have studied the chemical functionalization of TH-carbon by introducing fluorine atoms with various configurations such as single- and double-sided fluorination. Using first-principles density-functional theory (DFT) calculations, we have studied the stability of TH-carbon and its fluorinated derivatives from the energetic, dynamic, thermal, and mechanical aspects with the results of binding energy, phonon band structure, thermal stability, and elastic constants, respectively. Our results showed that, depending on the fluorine coverage, we examined the tunability of the electronic band gap and the direct-indirect-direct band gap transitions. We studied the effect of fluorination on the phononic gap in TH-carbon since the gap in the frequency spectrum plays an important role on the thermal properties. We found that the phonic gap can be controlled by fluorination. A decrease in the specific heat capacity was observed with increasing fluorine coverage, which is useful for nanoscale engineering of heat management. The fluorination is found to reduce the in-plane stiffness and Young's modulus but it increases the ultimate strength.

## METHODOLOGY

The first-principles calculations and *ab initio* molecular dynamics (AIMD) simulations are performed using density-functional theory (DFT) method as implemented in the Vienna Ab initio Simulation Package (VASP).[27] For the exchange correlation energy functional, the projector-augmented wave function (PAW) method[28,29] with the Perdew−Burke−Ernzerh (PBE)[30] of generalized gradient approximation (GGA) was applied. To achieve a higher precision in our electronic band structure calculations, we adopted the Heyd−Scuseria−Ernzerhof (HSE)[31,32] hybrid functional, constructed by mixing 25% of nonlocal Fock exchange with 75% of PBE exchange and 100% of PBE correlation energy instead.

In our DFT calculations, a vacuum region of 20 Å along the out-of-plane direction was included since periodic boundary conditions were applied in all three dimensions. A Γ-centered *k*-mesh 24 × 24 × 1 was used for all geometry optimization and electronic band structure calculations, respectively. A plane-wave kinetic energy cutoff of 520 eV was employed. In the energy minimization using the conjugate gradient method, structure relaxations were performed without any symmetry constraint. The total energy of all geometries was calculated with high precision and converged to $10^{-6}$ eV/atom. The lattice constants and the atom coordinates were relaxed until the interatomic forces were less than $10^{-2}$ eV/Å.

To calculate the binding energy ($E_b$) of the fluorine atom(s) on TH-carbon as a function of *x*, where *x* is the concentration of F in $CF_x$, the following expression is used

$$E_b = \frac{(E_{\text{TH-carbon}} + nE_F - E^x_{\text{TH-carbon/nF}})}{n} \quad (1)$$

where $E_{\text{TH-carbon}}$, $E_F$, and $E^x_{\text{TH-carbon/nF}}$ are the total energies of pristine TH-carbon, an isolated fluorine atom(s), and the fluorinated TH-carbon with a *x* concentration of F, respectively, and *n* is the number of attached F atoms per unit cell for given *x*. $E_b > 0$ implies the adsorption is energetically favorable.

In AIMD simulations, the convergence criterion of total energy is set as 0.1 meV. The calculations were performed in 4 × 4 × 1 supercells with the temperature starting from 300 K and then gradually being increased up to 900 K. Temperature


https://dx.doi.org/10.1021/acs.jpcc.9b12022
J. Phys. Chem. C 2020, 124, 8225−8235

**Table 1. Calculated Structure Parameters of TH-Carbon and Its Fluorinated Derivatives in 2 × 2 Supercell**[a]

| structure | Θ | $a$ | $b$ | $h$ | $d_{C_1^F-C_1}$ or $d_{11}$ | $d_{C_1^F-C_2}$ or $d_{12}$ | $d_{C_1^F-F}$ | $\theta$ | $E_b$ | $M$ | $E_g$(PBE/HSE06) | type |
|---|---|---|---|---|---|---|---|---|---|---|---|---|
| TH-carbon | 0 | 4.533 | 6.107 | 0.58 | 1.34 | 1.54 | | 123.9 | | 0 | 1.62/2.63 | direct |
| F/TH-carbon | 2 | 4.531 | 6.102 | 0.74 | 1.49 | 1.60 | 1.41 | 114.6 | 3.25 | 1.0 | | metallic |
| $C_6F$(s) | 17 | 4.503 | 6.085 | 0.72 | 1.56 | 1.59 | 1.39 | 118.1 | 4.07 | 0 | 1.98/3.06 | indirect |
| $C_3F$(s) | 33 | 4.536 | 6.090 | 0.70 | 1.55 | 1.58 | 1.37 | 118.2 | 3.85 | 0 | 2.25/3.39 | indirect |
| $C_3F_2$(d) | 67 | 4.531 | 6.126 | 0.81 | 1.57 | 1.57 | 1.38 | 118.3 | 3.79 | 0 | 2.83/3.85 | direct |

[a]Here, the fluorine concentration (Θ) in %, the unitcell lattice constants $a$ and $b$, buckling height $h$, bond lengths between $C1^F$ and $C_1$ atoms $d_{C_1^F-C_1}$ or $d_{11}$, and between $C1^F$ and $C_2$ atoms $d_{C_1^F-C_2}$ or $d_{12}$, between F and $C1^F$ atoms $d_{C_1^F-F}$ in Å, and the bond angle between carbon atoms ($C_1$—$C_1^F$—$C_2$) $\theta$ in °, the binding energy $E_b$ in eV/F, the total magnetic moment $M$ in $\mu_B$, the electronic band gap energy $E_g$ in eV are presented for all the considered structures.

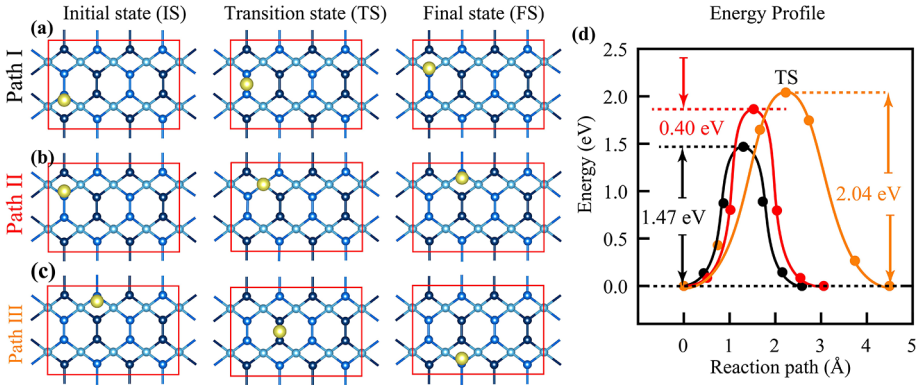


**Figure 2.** Energy pathways for a single F atom on 2 × 2 TH-carbon supercell along the three different reaction pathways, (a) Path I, (b) Path II, and (c) Path III where the relaxed atomic configurations of the IS, TS, and FS are illustrated. (d) Diffusion energy barrier and MEP along each considered path.

control was achieved using Nose—Hover thermostat.[33−35] The time step used for the integration of equations of motion was set to $t$ = 1 fs, and the total time for the simulation was 2.5 ps.

To explore the dynamics stability of all the TH-carbon systems, the phonopy software[36] is used in combination with VASP to produce phonon frequencies and obtain the second-order force constants (FCs). The phonon band calculations for all the considered systems were performed in a 4 × 4 × 1 supercell with 3 × 3 × 1 $k$- mesh with high accuracy (the convergence criterion of total energy was set as $1 \times 10^{-8}$ eV)

To examine the diffusion barrier property of the single F atom on TH-carbon, the climbing-image nudged elastic band (NEB) method[37] was used to find minimum energy paths (MEP) and transition states (TS) given from the initial state (IS) and final state (FS). The five linearly interpolated images between two energetic sites (IS and FS) for single F atom diffusion were taken. All of the images were relaxed until the maximum force acting on an atom was less than 0.01 eV $Å^{-1}$. The maxima on the MEP are saddle points and then verified to be true TS.

To examine the chemical bonding environment for $sp^2$- and $sp^3$-hybridized carbon atoms, the electron localization function (ELF) as an ideal visualization tool[38] is calculated using the Kohn—Sham DFT orbitals.

## RESULTS AND DISCUSSION

**Atomic Structure and Energetics.** Contrary to graphene (where all carbon atoms are equivalent to $sp^2$-hybridization), there are two chemically nonequivalent carbon atoms in TH-carbon. Its structure consists of a three-atom thickness of the planar carbon membrane with a perfectly ordered arrangement of tetra-hexa (TH-) carbon rings with 12 atoms in unitcell where there are eight $sp^2$- and four $sp^3$-hybridized carbon atoms, namely $C_1$ and $C_2$, respectively. The top and side views of the TH-carbon structure are shown in Figure 1a. The calculated lattice parameters for pristine TH-carbon are given in Table 1. The obtained lattice parameters of pristine TH-carbon are in good agreement with the previous calculation.[15]

Considering the possible experimental realization of TH-carbon (were not synthesized yet), we evaluated the formation energy difference of pristine TH-carbon. The formation energy difference $\Delta E_f$ per C atom was calculated using the equation

$$\Delta E_f = E_{2D} - E_{3D}$$

where $E_{2D}$ and $E_{3D}$ are per C atom energies of 2D and the reference bulk materials, respectively. The low energy difference indicates that the 2D materials can easily form from their bulk counterparts. Looking at previous studies, the $\Delta E_f \leq 200$ meV/C implies that the 2D materials can be synthesized as free-standing such as in graphene, BN, and $MoS_2$.[1,39−41] The $\Delta E_f$ for other 2D materials, such as graphdiyne,[42] silicene,[43] and ZnO,[44] which have been synthesized experimentally on the substrate, is higher than 200 meV/C.[45] For instance, the $\Delta E_f$ of 823 meV/C graphdiyne was experimentally synthesized on the copper surface.[42] For TH-carbon, we calculated the $\Delta E_f$ to be about 920 meV/C, hence TH-carbon would require a suitable substrate on which it can be experimentally realized. The lower energy and robust stability (based on dynamical, thermal, and mechanical stability) is evidence of the possibility of the existence of TH-carbon.

Because of the special atomic configuration of TH-carbon, we tried several different positions to adsorb a F atom on a 2 × 2 TH-carbon supercell (the red stars in Figure 1a). Our results


https://dx.doi.org/10.1021/acs.jpcc.9b12022
J. Phys. Chem. C 2020, 124, 8225−8235

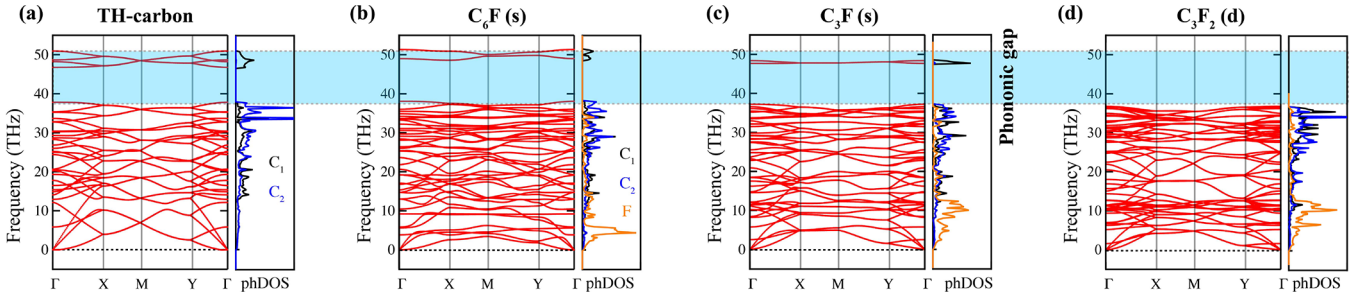


**Figure 3.** Phonon band structures and corresponding atom-resolved PhDOS of (a) pristine TH-carbon, (b) $C_6F$(s), (c) $C_3F$(s), and (d) $C_3F_2$(d). Here, the band structures are plotted along the high-symmetric $q$-point paths: Γ(0, 0), X(1/2, 0), M(1/2, 1/2), Y(0, 1/2), Γ(0, 0). The shaded blue regions indicated the phononic gaps. Note that, all the phonon modes of TH-carbon and its fluorinated derivatives are totally positive, indicating their dynamic stability.

indicated that the most stable adsorption site is the top of the $sp^2$-hybridized carbon atom ($C_1$) with the binding energy of 3.25 eV. This configuration is referred as F/TH-carbon. The F atom hybridizes the unhybridized p orbital of the $C_1$ atom, and making the $C_1$ atom to $sp^3$-hybridized (denote as $C_1^F$), which causes a local atomic distortion (see Figure S1 of Supporting Information). The $C_1$—$C_1^F$—$C_2$ angle decreased from 123.9° to 114.6°, which is close to that of fluorinated graphene (110.84°) and ideal $sp^3$ (109.47°) hybridizations.[18] The results of the structural parameters for the F/TH-carbon are summarized in Table 1.

We next studied the single F atom diffusion on TH-carbon using the NEB algorithm. Three typical migration pathways (namely, Path I, Path II, and Path III), as shown in Figure 2, were optimized. The converged MEP including IS, FS, and TS for each considered path are presented in Figure 2a−c. The migration energy barriers for the single F atom on TH-carbon along the Path I, Path II, and Path III are very high at about 1.47, 1.87, and 2.04 eV, respectively, (Figure 2d). We conclude the low possibility of fluorine migration occurs from one energetic site ($C_1$) to another and the F atom strongly binds to an $sp^2$-hybridized carbon atom.

We further analyzed the adsorption of two fluorine atoms on a 2 × 2 supercell. With two adatoms, several different configurations are possible. Here, we discuss the configurations where the adsorption on the next nearest neighbor sites (namely 2F/TH-carbon-1 and 2F/TH-carbon-2) and the nearest neighbor site (2F/TH-carbon-3) are in the same plane (see Figure S2 of Supporting Information). Structural optimization indicates that the binding energy of the 2F/TH-carbon-1 and 2F/TH-carbon-2 is 2.98 and 3.09 eV, respectively, and is reduced compared to the F/TH-carbon due to the repulsive interaction of the two fluorine atoms. Instead, for 2F/TH-carbon-3, namely "ortho-dimer" configuration, the binding energy is increased by 0.86 eV. Similarly, the ortho-dimer configurations on graphene lattice exhibit strong stability as compared to other configurations of two fluorine atoms.[25] Therefore, the two fluorine atoms prefer to bind to two adjacent $sp^2$-hybridized carbon ($C_1$) atoms with the strong binding energy of 4.11 eV (see Figure S2d of Supporting Information). We now turn to the adsorption of two fluorine atoms on the TH-carbon unit cell where the concentration of the fluorine atoms, Θ, is 17%. This configuration referred to $C_6F$(s) is presented in Figure 1b. The calculated binding energy is about 4.07 eV, which is 0.04 eV lower that that in the 2 × 2 supercell of TH-carbon due to the interactions between periodic images of the adatoms. The distance between the two fluorine atoms in the $C_6F$(s) is found to be 2.46 Å. We observed that the fluorine adsorbed carbon atoms move simultaneously in the same direction (Figure S1c of Supporting Information). However, one can easily see that the atomic distortions are negligible for the second and third neighbors of the fluorine-bonded carbon atoms. Considering the negligible atomic distortions and the high binding energy, we conclude that extra stability is gained through the fluorine pairing. The electrons that were previously in the unhybridized p orbitals are now localized the $C_1$—F $\sigma$-bond (see the big red regions in Figure 1b, lower panel). The $d_{C_1^F-C_1}$ increased from 1.33 to be 1.56 Å, which is close to the standard value of $sp^3$ C—C bonds (1.54 Å).[46] Another possible configuration is the Θ = 17% case; we studied two fluorine atoms adsorbing two adjacent $sp^2$-hybridized carbon atoms on opposite sides of the TH-carbon unitcell (see Figure S3 of Supporting Information). The results of the phonon band calculations indicated the structure is dynamically stable. We then attempt to test the other stability criteria (thermal stability). The potential energy diagram and the atomic configurations of the AIMD results at 900 K revealed that the structure is thermally unstable. For the partially fluorinated TH-carbon, we tried to explore another possible fluorinated derivatives in the unitcell. However, they did not pass the stability tests (see Figure S4 of Supporting Information).

With increasing fluorine coverage, we studied the case of single- and double-sided full fluorination of TH-carbon. For the single-sided full fluorination, all the $sp^2$-hybridized carbon atoms on the one-side of TH-carbon are fluorinated, where the concentration of fluorine, Θ, is 33%. This configuration, referred to as $C_3F$(s), is presented in Figure 1c. The distance between the fluorine atoms in $C_3F$(s) is slightly decreased to 2.37 Å, which leads to a reduction in the binding energy due to the repulsive interaction of two fluorine atoms attached to TH-carbon. The obtained binding energy is 3.85 eV/F, which is 0.22 eV lower than that of $C_6F$(s). One can easily see that the $C_1$—$C_1$ bonds on one side of TH-carbon are pure $\sigma$-bond (Figure 1c, lower panel). In the case of the double-sided full fluorination of TH-carbon (Θ = 67%), all the $sp^2$-hybridized carbon atoms are fluorinated on both sides of the TH-carbon sheet (Figure 1d). This configuration is denoted as $C_3F_2$(d). The covalency in $C_3F_2$(d) is almost fully $sp^3$, and the C—C bonds are pure $\sigma$-bonds. The distance between the fluorine atoms in $C_3F_2$(s) is found to be 2.36 Å. The binding energy is found to be 3.79 eV, which is 0.06 eV lower than that of $C_6F$(s).

As a result, the fluorination of TH-carbon increases the system mass, membrane thickness, chemical bond length, and changes the nature of bonds, consequently resulting in change in the


https://dx.doi.org/10.1021/acs.jpcc.9b12022
J. Phys. Chem. C 2020, 124, 8225−8235

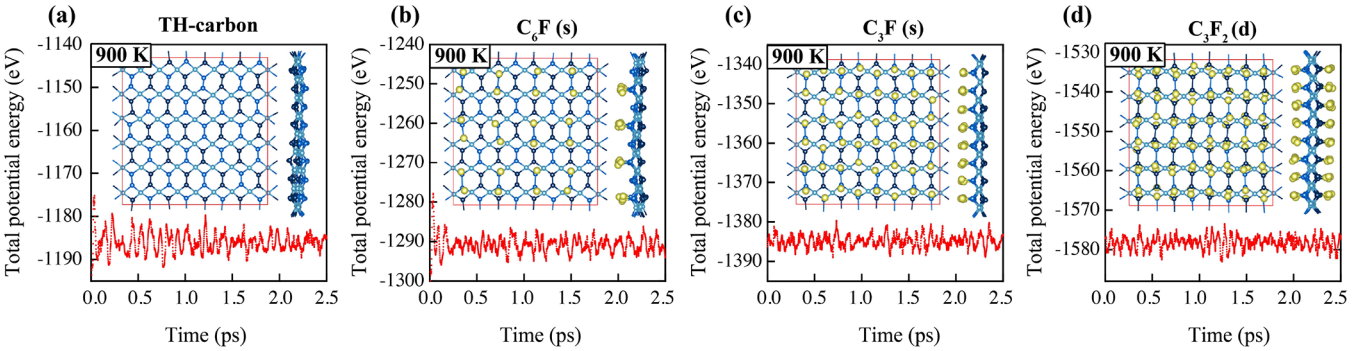


**Figure 4.** Fluctuations of total potential energy of (a) pristine TH-carbon, (b) $C_6F$(s), (c) $C_3F$(s), and (d) $C_3F_2$(d) during the AIMD simulations at $T$ = 900 K. The insets are snapshots of the atomic structures at the end of simulations.

vibrational modes, thermal, mechanical, and electronic properties of the 2D sheets.

**Dynamic Stability and Phonon Properties.** We turn now to study the dynamical stability of pristine TH-carbon and its fluorinated derivatives by performing the *ab initio* lattice dynamics. The calculated phonon frequencies of all modes as a function of the *k*-points in the BZ are presented in Figure 3. The absence of imaginary modes in the phonon calculation shows that the pristine TH-carbon and its fluorinated derivatives are dynamically stable.

The phonon spectra of the pristine TH-carbon, $C_6F$(s), $C_3F$(s), and $C_3F_2$(d) have three distinct acoustic phonon branches. The transverse in-plane (TA) and longitudinal in-plane (LA) exhibit linear dispersion near the Γ-point, whereas the out-of-plane (ZA) mode shows a quadratic dispersion when $q$ approaches zero. We observed that fluorination leads to the dense phonon modes located in the frequency above acoustic modes since the formation of the C—F bond introduces new phonon modes. The low frequency of C—F phonon modes can be explained by the atomic mass of fluorine atoms. Fluorine has a high atomic mass, and the vibration frequency is inversely proportional to the effective mass of the system.

More interestingly, one can see from Figure 3 that there exists a complete phononic gap vibration range of 40−50 THz in the phonon spectra of pristine and partially fluorinated TH-carbon sheets. After a careful analysis, the corresponding atom resolved phonon density-of-the states (PhDOS), high frequency modes around 50 THz come mainly from $sp^2$-hybridized carbon atoms ($C_1$). In Figure 3 (see sky blue region), the phonon branches at around 40−50 THz are gradually annihilated by increasing fluorination. We noted that the surface modification by fluorination breaks the double bonds between $C_1$ atoms, which result in the disappearance of the high-frequency modes. As a result, the phononic gap of the TH-carbon can be tuned by fluorination, which could be useful for thermoelectric devices since the existence of the phononic gap can limit the contribution of phonon in thermal properties.

**Thermal Stability and Properties.** To further examine the thermal stability of TH-carbon and its fluorinated derivatives, we performed the AIMD simulations using canonical ensemble at 900 K for $t$ = 2.5 ps with a time step d$t$ = 1 fs. We simulated a 4 × 3 supercell to reduce the periodic constraints and explore possible structure reconstruction. The fluctuations of the total potential energies and atomic configurations at the end of the AIMD simulations for pristine TH-carbon, $C_6F$(s), $C_3F$(s), and $C_3F_2$(d) are presented in Figure 4. The fluctuations are caused by the thermal oscillations of the atoms around their equilibrium positions. The average values of potential energy for the considered systems remain nearly constant during the AIMD simulations. The AIMD simulation approves thermal stability due to the occurrence of no structural changes at 900 K for 2.5 ps. Even if the present simulation time is very short due to the computational limit in the AIMD calculations, this result at least indicates that the structure is stable with respect to the thermal shock.

The fluorination of TH-carbon increases the system mass and membrane thickness and the chemical bond length and consequently changes the vibrational modes of the 2D system. To examine the functionalization of TH-carbon on the thermal properties, we investigated the constant-volume specific heat ($C_V$) and the vibrational entropy ($S$) of TH-carbon and its fluorinated derivatives within harmonic approximation. Using the PhDOS, the $C_V$ and $S$ are calculated using the following equations

$$C_V(T) = k_B \sum_{q^i} \left(\frac{\hbar\omega_{q^i}}{k_B T}\right)^2 \frac{\exp\left(\frac{\hbar\omega_{q^i}}{k_B T}\right)}{\left(\exp\left(\frac{\hbar\omega_{q^i}}{k_B T}\right) - 1\right)^2} \quad (2)$$

$$S = -\frac{\partial F}{\partial T} = \frac{1}{2T}\sum_{q^i} \hbar\omega_{q^i} \coth\left(\frac{\hbar\omega_{q^i}}{2k_B T}\right) - k_B \sum_{q^i} \ln\left(2\sinh\left(\frac{\hbar\omega_{q^i}}{2k_B T}\right)\right) \quad (3)$$

where **q** is the wave vector, $\omega_{q^i}$ is the phonon frequency at **q** with phonon mode $i$, $T$ is the temperature, $k_B$ is the Boltzmann constant, and $\hbar$ is the reduced Planck constant. The variation of $C_V$ and the $S$ with temperature for pristine TH-carbon, $C_6F$(s), $C_3F$(s), and $C_3F_2$(d) are presented in Figure 5. It is easy to observe from the graph as shown in Figure 5a that the $C_V$ for the pristine TH-carbon as well as fluorinated TH-carbon reaches a constant value, approaching Dulong−Petit limit. We note that TH-carbon has a high specific capacity and hence can be used for storing and transferring energy. The $C_V$ of pristine TH-carbon and its fluorinated derivatives are almost the same up to 300 K while they become different at higher temperatures. Hence, the influence of functionalization on the $C_V$ of TH-carbon was detected at high temperatures. The results showed that the fluorination reduces the $C_V$ of TH-carbon since the fluorinated TH-carbon systems have higher effective mass than that of pristine TH-carbon high molar mass of fluorine. The $S$ of the fluorinated TH-carbon is close to that for pristine TH-carbon (Figure 5b).

**Mechanical Stability and Properties.** We examined the mechanical stability of pristine TH-carbon and its fluorinated derivatives by the following elastic stability criteria of 2D


https://dx.doi.org/10.1021/acs.jpcc.9b12022
J. Phys. Chem. C 2020, 124, 8225−8235

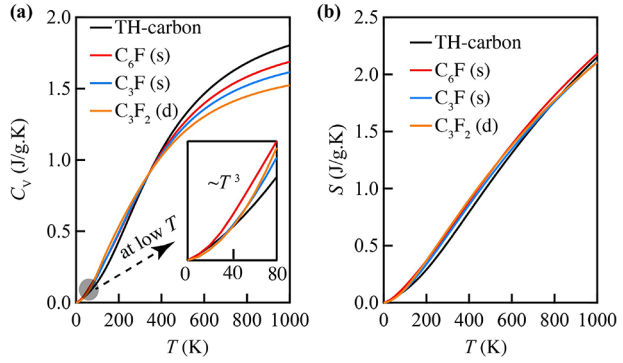


**Figure 5.** (a) Variation of specific heat at $C_V$ with respect to $T$ for pristine TH-carbon (in black), $C_6F$(s) (in red), $C_3F$(s) (in sky blue), and $C_3F_2$(d) (in orange). The inset is the $C_V$ at low temperature (below 80 K). (b) Variation of $S$ with respect to $T$.

crystals:[47] $C_{11}C_{22} - C_{12}^2 > 0$ and $C_{66} > 0$. Here, $C_{11}$, $C_{22}$, $C_{12}$, and $C_{66}$ are elastic stiffness coefficients, which are derived from the second derivative of total energy with respect to the in-plane strain (uniaxial, biaxial, and shear strain conditions) at equilibrium area (Figure 6a–d, left panels).

Here, we applied a series of lateral compressive/tensile strain ranging from −2.5% to 2.5% along the corresponding $x$- and $y$-directions to equilibrated TH-carbon and its fluorinated derivatives and calculated the total energies for each strain case. Results from applied strain versus strain energy relationships are presented in Figure 6a–d, left panels. As a benchmark, our calculated $C_{ij}$ values for the pristine TH-carbon are found to be $C_{11}$ = 287.03 N/m and $C_{22}$ = 280.82 N/m, agreeing well with the previous result.[15] The calculated elastic stiffness coefficients of TH-carbon and its fluorinated derivatives are listed in Table 2. Clearly, the obtained elastic stiffness coefficients ($C_{ij}$) satisfy the elastic stability criteria, suggesting that the pristine TH-carbon and its fluorinated derivatives are mechanically stable.

The obtained elastic stiffness coefficients were then used to calculate the mechanical response of the TH-carbons such as Young's modulus ($Y$), shear modulus ($G$), and Poisson's ratio ($P$). Young's moduli of pristine TH-carbon along the $a$ and $b$ lattice directions are calculated as $Y_a$ = 286.12 N/m and $Y_b$ = 279.88 N/m, respectively. It is important to compare the mechanical properties of the pristine TH-carbon with those of PG since PG possesses robust mechanical stability and outstanding mechanical properties, and TH-carbon was constructed from PG by applying Stone–Wales transformations. It is noted that the Young's modulus of TH-carbon is found to be higher than that of PG (263.8 N/m),[14] and fluorination slightly reduces the Young's modulus. Young's modulus for the $C_6F$(s), $C_3F$(s), and $C_3F_2$(d) is 277.86, 282.50, and 270.55 N/m, respectively, which are still comparable to that of pristine TH-carbon (286.12 N/m) and higher than that of fluorinated PG (239.12 N/m).[48] The slight reduction of Young's modulus can be attributed to the difference of the bond order and bond type between the pristine TH-carbon and the fluorinated TH-carbon. Likewise, we found that the shear modulus of TH-carbon is reduced by fluorination. The Poisson's ratio of pristine and fluorinated TH-carbon is found to be positive (see Figure 6a–d, middle panels).

Next, we calculated the ultimate strength for pristine TH-carbon and its fluorinated derivatives. The results are presented in Figure 6a–d, right panels). As shown in the stress versus strain curve for the considered systems, the in-plane stress monotonically increases to reach the maximum stress with increasing applied tensile strain. The calculated strain at the maximum strength is 20% for pristine TH-carbon, which is almost same with that of PG (21%).[14] The ultimate strength value of the $C_6F$(s), $C_3F$(s), and $C_3F_2$(d) is about 15.2, 20.5, and 22.1%, respectively. As a result, the ultimate strength reduces with partial fluorination ($C_6F$(s)), whereas it increases with the case of full fluorination on the single- and double-sided TH-carbon ($C_3F$(s) and $C_3F_2$(d)).

**Electronic Properties.** To examine the electronic properties of pristine TH-carbon and its fluorinated derivatives, we calculated their electronic band structure, the atom/orbital-projected density of states (PDOS), the charge distribution at the highest energy of valence bands (VBM), and the lowest energy of conduction bands (CBM), and the electron localization function (ELF). The results of electronic band structure calculations are depicted in Figure 7 and Figure 8. The charge densities and the PDOS are presented in Figure S5 and Figure S6 of Supporting Information, respectively. A summary of the results for the electronic properties of these systems is also presented in Table 1.

The pristine TH-carbon is a direct band gap semiconductor as its the VBM and CBM are both located at Γ-point in the rectangular Brillouin zone as shown in Figure 8a. The calculated band gap is about 1.62 eV at the PBE level. Because of the band gap underestimation of the PBE functional, we used the hybrid HSE06 functional to get more accurate results. The band gap changes to 2.63 eV. The isosurfaces of band decomposed charge density for the VBM and CBM at the Γ-point of the band structure are plotted to visualize the electron localization. The results showed that the electrons are predominantly localized on $sp^2$-hybridized carbon atoms ($C_1$), which were further confirmed by the PDOS results. The electronic states near the Fermi level are derived mainly from the $p_z$ orbital of $C_1$ atoms, which are presented in Figure S6a of Supporting Information. All these results for pristine TH-carbon are in good agreement with the previous calculation.[15]

We then studied how fluorine atoms affect the electronic properties of the TH-carbon. For the single F atom adsorbed on TH-carbon (F/TH-carbon), the results of Bader charge analysis, the electronic band structure, the PDOS, and the ELF plot of F/TH-carbon are presented in Figure 7. The calculated Bader charge values on F and $C_1^F$ atoms indicated that upon fluorine adsorption the charge transfer occurs from $C_1^F$ to the F atom at about 0.54 e due to high electronegativity of the F atom (Figure 7a). According to the electronic band structure, we observed that the VBM of the spin-up band structure passes through the Fermi level ($E_F$), indicating that F/TH-carbon is metallic (Figure 7b). However, the spin-down electronic band structure exhibits a semiconductor behavior. Analysis of the spin projected density of states revealed that the spin-up and spin-down states are slightly aligned near the Fermi level, which induces the system to the spin polarization with a magnetic moment of 1.0 $\mu_B$. To understand the main contribution of this inducing effect, we analyze the PDOS of F/TH-carbon (Figure 7c). The $p_z$ orbital of the $C_1^F$ almost disappeared when compared with that of another carbon atom ($C_1$*). We note that the main contribution comes from the $p_z$ orbital of the $C_1^F$. As a result, the electrons that were previously in the unhybridized p orbital of the $C_1$ atom in pristine TH-carbon are now localized (Figure 7d). The adsorption of the F atom on TH-carbon can be considered as a local defect since it locally removes the $p_z$ orbitals from the bonded $sp^2$-hybridized carbon, resulting in an


https://dx.doi.org/10.1021/acs.jpcc.9b12022
J. Phys. Chem. C 2020, 124, 8225−8235

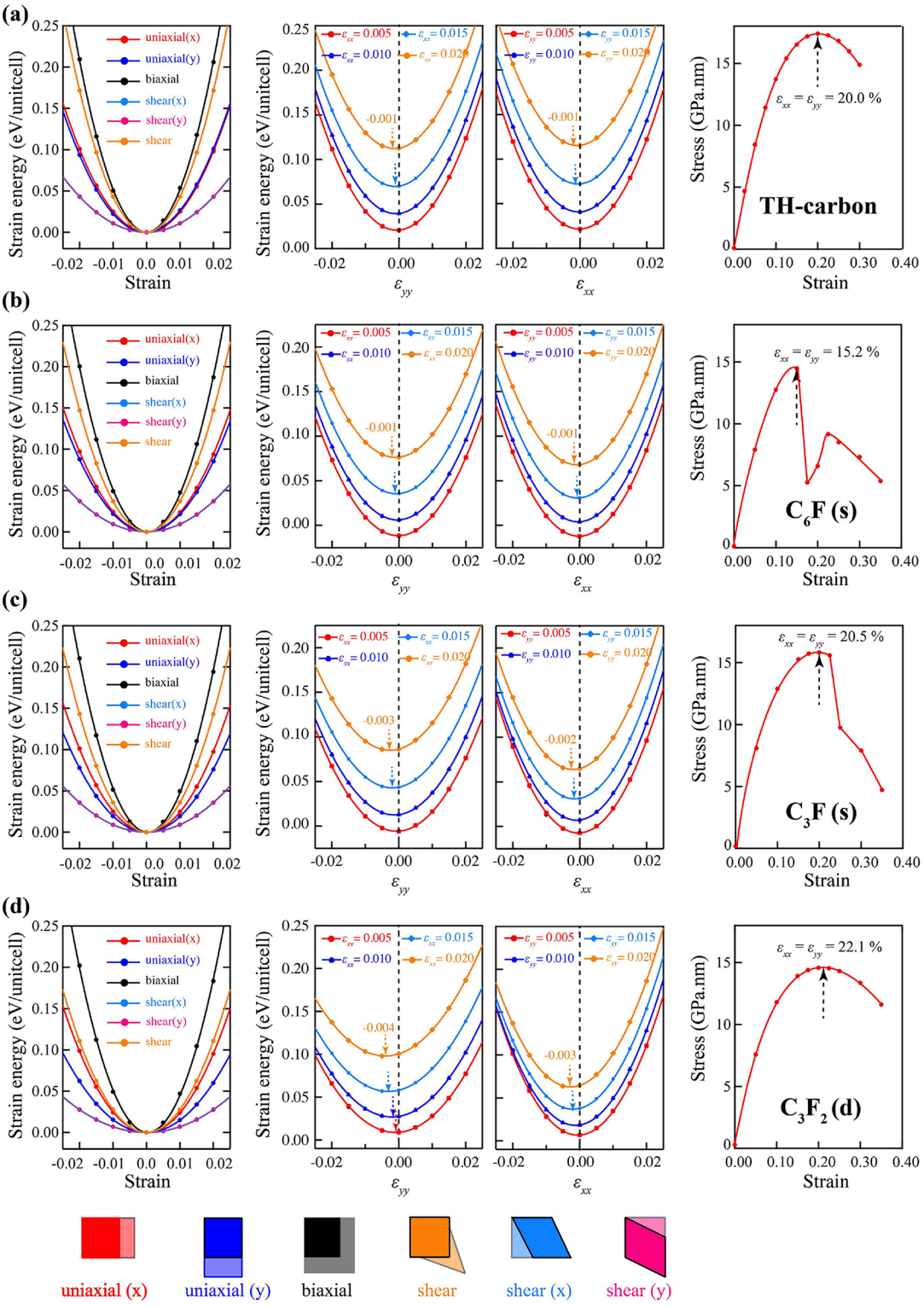


**Figure 6.** Strain-energy (left and middle) and strain−stress (right) relationship of (a) pristine TH-carbon, (b) $C_6F$(s), (c) $C_3F$(s), and (d) $C_3F_2$(d). In the right panels, the ultimate strength value for each considered system is depicted by the dashed arrows.

asymmetric bonding environment and a distortion of the unhybridized p orbitals, and giving a metallic behavior. The $C_6F$(s), $C_3F$(s), and $C_3F_2$(d) systems maintained the semiconductor characteristic with the absence of the asymmetric bonds.

Referring to Figure 8, the electronic band structure of TH-carbon and its fluorinated derivatives shows their semiconductor behavior and indicates that the electronic bands of the TH-carbon are modified by fluorination. This can be attributed to the redistribution of charge density (Figure S5 of Supporting Information). The charge density distributions of the band edge states for the TH-carbon and its fluorinated derivatives were analyzed as well and presented in Figure 8, lower panel. The analysis of the PDOS at the Fermi level reveals that the VBMs



https://dx.doi.org/10.1021/acs.jpcc.9b12022
J. Phys. Chem. C 2020, 124, 8225−8235

**Table 2. Calculated Elastic Stiffness Constants $C_{ij}$ in N/m, Young's Modulus ($Y$) in N/m, and Poisson's Ratios ($P$) along *a* and *b* Lattice Directions of TH-Carbon and Its Fluorinated Derivatives**

| | $C_{11}$ | $C_{22}$ | $C_{12}$ | $C_{66}$ ($G$) | $Y_a$ | $Y_b$ | $P_a$ | $P_b$ |
|---|---|---|---|---|---|---|---|---|
| TH-carbon | 287.03 | 280.82 | 16.21 | 123.99 | 286.12 | 279.88 | 0.06 | 0.06 |
| $C_6F(s)$ | 278.89 | 252.75 | 16.90 | 107.29 | 277.86 | 251.62 | 0.06 | 0.07 |
| $C_3F(s)$ | 287.49 | 222.67 | 37.87 | 103.54 | 282.50 | 216.23 | 0.13 | 0.17 |
| $C_3F_2(d)$ | 279.50 | 176.02 | 50.02 | 79.81 | 270.55 | 161.81 | 0.18 | 0.28 |

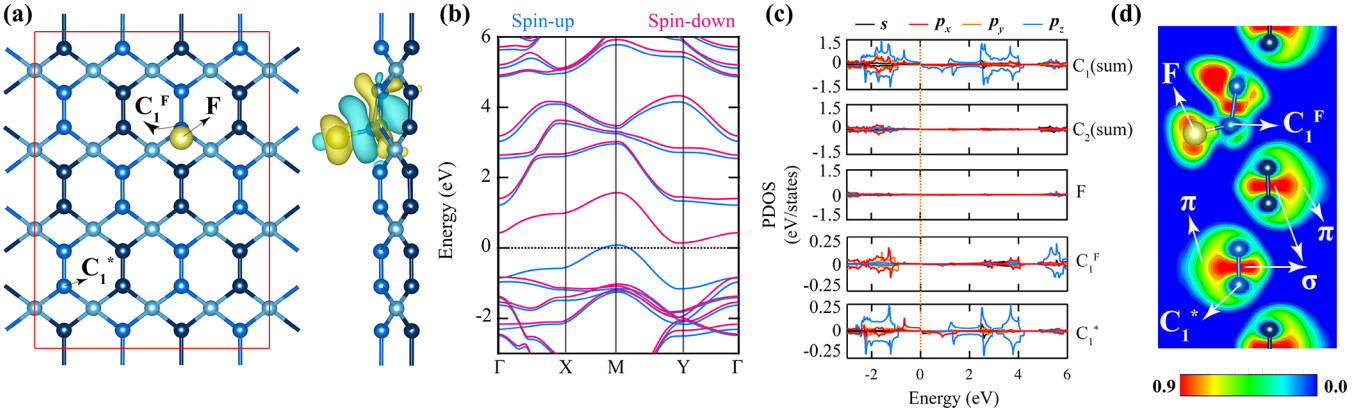


**Figure 7.** (a) Charge density difference plot of F/TH-carbon. Yellow and cyan isosurface represent electron accumulation and electron depletion region, respectively. (b) Calculated spin-polarized band structures compound for spin-up (in sky blue) and spin-down (in light pink) electrons. (c) The PDOS and (d) ELP plot of F/TH-carbon.

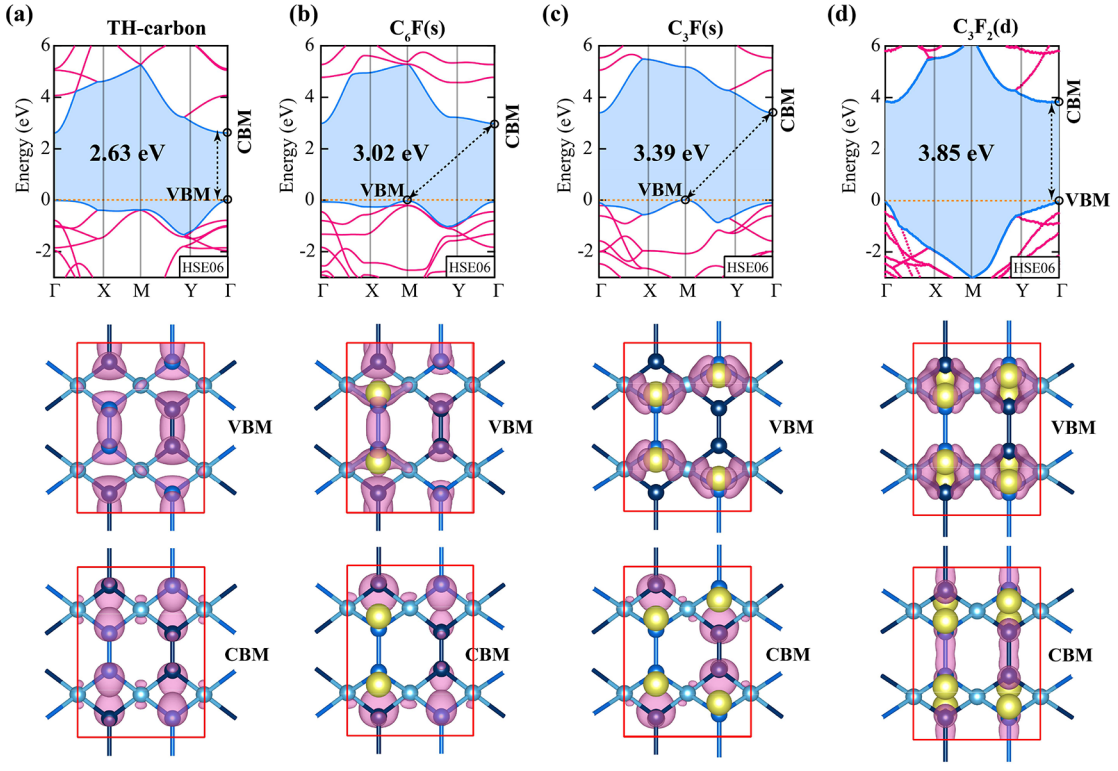


**Figure 8.** Electronic band structure and charge distribution at the highest energy of valence bands (VBM) and the lowest energy of conduction bands (CBM) of (a) pristine TH-carbon, (b) $C_6F(s)$, (c) $C_3F(s)$, and (d) $C_3F_2(d)$. The Fermi level is shifted to 0 eV and is shown by the dashed orange line. The isovalue is 0.01 eÅ$^3$.

and CBM are mainly contributed by the $p_z$ orbitals of $C_1$ atoms (see Figure S6), which are also confirmed by calculating the band-decomposed charge density distributions. Thus, the $sp^2$ hybridized carbon atoms ($C_1$) play an important role to modify the electronic band structure. Now we will analyze the physical origin of the direct−indirect−direct transition of the band gaps. For the single-sided fluorination case, the electronic band structures of the $C_6F(s)$ and $C_3F(s)$ indicated that the systems become an indirect gap material due to the VBM transition (the VBM state is located at M-point in the reciprocal space while the



https://dx.doi.org/10.1021/acs.jpcc.9b12022
J. Phys. Chem. C 2020, 124, 8225−8235

CBM is still located at Γ-point). However, the existence of the sub-VBM at Γ-point is very close to true VBM in energy (around 0.07 eV), and the $C_6F(s)$ and $C_3F(s)$ can also be considered as a quasi-direct bandgap semiconductor. The band gap value of the $C_6F(s)$ and $C_3F(s)$ is about 3.02 and 3.39 eV, respectively. This indicates that increasing the F concentration (resulting in increasing the ratio of $sp^3$-hybridized carbon atoms) on TH-carbon leads to an increased band gap.

For a full fluorination case ($C_3F_2(d)$), all the carbon atoms are $sp^3$ as shown in Figure 1d, and electron bonds are saturated with fluorine atoms, demonstrating the insulator characteristics. The $C_3F_2(d)$ exhibits a wide direct bandgap semiconductor with 3.85 eV due to the rigid upshift of the CBM. The VBM turns to Γ-point, causing the indirect−direct transition. The full fluorinated system possesses more symmetric and localized electron distribution with pure $\sigma$-bonds. The band gap significantly opened when compared to that of the pristine TH-carbon (2.63 eV). The band gap value is lower than that of fluorinated graphene (4.74−5.10 eV)[48,49] and fluorinated PG (4.78)[48] using HSE06 hybrid functional. All these results indicated that the ratio of $sp^2$- and $sp^3$-hybridized carbon atoms govern the electronic structure of TH-carbon. In the final discussion, we summarized the relation between the electronic bandgap and fluorination concentration. Figure 9 shows that the relation is linear. The band gap of TH-carbon can be tuned by fluorination.

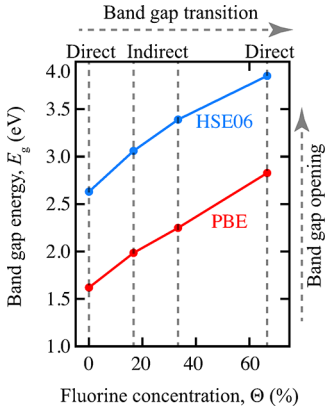


**Figure 9.** Electronic band gap energies as a function of F concentration in fluorinated TH-carbon sheets. The red and blue circles are the PBE and the hybrid HSE06 functional value of the electronic band gap, respectively.

## CONCLUSION

The most significant results of the present study show that the physical and chemical properties of TH-carbon can be manipulated by fluorination, which effectively designs the hybridization states of the carbon atoms. The results of phonon spectrum, AIMD simulations, and elastic constants results revealed that the pristine TH-carbon and its fluorinated derivatives are dynamically, thermally, and mechanically stable. Depending on the fluorine coverage, we examined the tunability of the phononic gap and electronic band gap. Moreover, the direct−indirect−direct band gap transitions were observed. We found that the phononic gap can be controlled by fluorination. A decrease in the specific heat capacity was observed with increasing fluorine coverage, which is useful for nanoscale engineering of heat management. The fluorination is found to reduce the in-plane stiffness and Young's modulus, but it increases the ultimate strength. These results suggest fluorination would enable the ability to tailor TH-carbon material for several interesting technological applications. Since these materials are expected to be stable, it should be possible to prepare them, for example, by controlled fluorination of TH-carbon, by exfoliation of the corresponding pristine materials, or exchange reactions starting from fluorinated TH-carbon as proposed for graphene.[5,49−52]

## ASSOCIATED CONTENT

### Supporting Information

The Supporting Information is available free of charge at https://pubs.acs.org/doi/10.1021/acs.jpcc.9b12022.

Picture of local distortion from side view for pristine TH-carbon and its fluorinated derivatives; Atomic configurations and binding energies of two F atoms on TH-carbon; Atomic configurations, AIMD results and phonon dispersion curves for unstable configurations of partially fluorinated TH-carbon (Θ = 17%); Atomic configurations and phonon dispersion curves for unstable configurations of partially fluorinated TH-carbon (Θ = 33%); The charge distribution of TH-carbon, $C_6F(s)$, $C_3F(s)$ and $C_3F_2(d)$; the PDOS of TH-carbon, $C_6F(s)$, $C_3F(s)$ and $C_3F_2(d)$ (PDF)

## AUTHOR INFORMATION

### Corresponding Authors

**Mehmet Emin Kilic** − *Computational Science Center, Korea Institute of Science and Technology, Seoul 136 791, Republic of Korea*; orcid.org/0000-0003-1814-5104; Email: mekilic@kist.re.kr

**Kwang-Ryeol Lee** − *Computational Science Center, Korea Institute of Science and Technology, Seoul 136 791, Republic of Korea*; Email: krlee@kist.re.kr

Complete contact information is available at: https://pubs.acs.org/10.1021/acs.jpcc.9b12022

### Notes

The authors declare no competing financial interest.

## ACKNOWLEDGMENTS

We gratefully acknowledge the support by the Nano Materials Research Program through the Ministry of Science and IT Technology under Project Number NRF-2016M3A7B4025402. The computing environment was prepared by Virtual Lab Inc.

## REFERENCES

(1) Novoselov, K. S.; Geim, A. K.; Morozov, S. V.; Jiang, D.; Zhang, Y.; Dubonos, S. V.; Grigorieva, I. V.; Firsov, A. A. Electric Field Effect in Atomically Thin Carbon Films. *Science* **2004**, *306*, 666−669.

(2) Okamoto, H.; Kumai, Y.; Sugiyama, Y.; Mitsuoka, T.; Nakanishi, K.; Ohta, T.; Nozaki, H.; Yamaguchi, S.; Shirai, S.; Nakano, H. Silicon Nanosheets and Their Self-Assembled Regular Stacking Structure. *J. Am. Chem. Soc.* **2010**, *132*, 2710−2718.

(3) Song, L.; Ci, L.; Lu, H.; Sorokin, P. B.; Jin, C.; Ni, J.; Kvashnin, A. G.; Kvashnin, D. G.; Lou, J.; Yakobson, B. I.; Ajayan, P. M. Large Scale Growth and Characterization of Atomic Hexagonal Boron Nitride Layers. *Nano Lett.* **2010**, *10*, 3209−3215.

(4) Baughman, R.; Eckhardt, H.; Kertesz, M. Structure-Property Predictions for New Planar Forms of Carbon: Layered Phases Containing sp 2 and sp Atoms. *J. Chem. Phys.* **1987**, *87*, 6687−6699.

(5) Sofo, J. O.; Chaudhari, A. S.; Barber, G. D. Graphane: A Two-dimensional Hydrocarbon. *Phys. Rev. B: Condens. Matter Mater. Phys.* **2007**, *75*, 153401.
(6) Cheng, S.-H.; Zou, K.; Okino, F.; Gutierrez, H. R.; Gupta, A.; Shen, N.; Eklund, P.; Sofo, J.; Zhu, J. Reversible Fluorination of Graphene: Evidence of a Two-dimensional Wide Bandgap Semiconductor. *Phys. Rev. B: Condens. Matter Mater. Phys.* **2010**, *81*, 205435.
(7) Ipek, S.; Kilic, M.; Mogulkoc, A.; Cahangirov, S.; Durgun, E. Semiconducting Defect-free Polymorph of Borophene: Peierls Distortion in Two Dimensions. *Phys. Rev. B: Condens. Matter Mater. Phys.* **2018**, *98*, 241408.
(8) Pekoz, R.; Konuk, M.; Kilic, M. E.; Durgun, E. Two-Dimensional Fluorinated Boron Sheets: Mechanical, Electronic, and Thermal properties. *ACS omega* **2018**, *3*, 1815−1822.
(9) Novoselov, K. S.; Geim, A. K.; Morozov, S.; Jiang, D.; Katsnelson, M. I.; Grigorieva, I.; Dubonos, S.; Firsov, A. A. Two-Dimensional Gas of Massless Dirac Fermions in Graphene. *Nature* **2005**, *438*, 197.
(10) Zhang, Y.; Tan, Y.-W.; Stormer, H. L.; Kim, P. Experimental Observation of the Quantum Hall Effect and Berry's Phase in Graphene. *Nature* **2005**, *438*, 201.
(11) Yan, J.-A.; Ruan, W.; Chou, M. Phonon Dispersions and Vibrational Properties of Monolayer, Bilayer, and Trilayer Graphene: Density-Functional Perturbation Theory. *Phys. Rev. B: Condens. Matter Mater. Phys.* **2008**, *77*, 125401.
(12) Kaner, R. B.; Gilman, J. J.; Tolbert, S. H. Designing Superhard Materials. *Science* **2005**, *308*, 1268−1269.
(13) Malko, D.; Neiss, C.; Vines, F.; Görling, A. Competition for Graphene: Graphynes with Direction-Dependent Dirac Cones. *Phys. Rev. Lett.* **2012**, *108*, 086804.
(14) Zhang, S.; Zhou, J.; Wang, Q.; Chen, X.; Kawazoe, Y.; Jena, P. Penta-graphene: A new carbon allotrope. *Proc. Natl. Acad. Sci. U. S. A.* **2015**, *112*, 2372.
(15) Ram, B.; Mizuseki, H. Tetrahexcarbon: A Two-Dimensional Allotrope of Carbon. *Carbon* **2018**, *137*, 266−273.
(16) Kilic, M. E.; Lee, K.-R. Tuning the Electronic, Mechanical, Thermal, and Optical Properties of Tetrahexcarbon via Hydrogenation. *Carbon* **2020**, *161*, 71−82.
(17) Elias, D. C.; Nair, R. R.; Mohiuddin, T. M. G.; Morozov, S. V.; Blake, P.; Halsall, M. P.; Ferrari, A. C.; Boukhvalov, D. W.; Katsnelson, M. I.; Geim, A. K.; Novoselov, K. S. Control of Graphene's Properties by Reversible Hydrogenation: Evidence for Graphane. *Science* **2009**, *323*, 610−613.
(18) Medeiros, P. V.; Mascarenhas, A. J.; de Brito Mota, F.; de Castilho, C. M. A DFT Study of Halogen Atoms Adsorbed on Graphene Layers. *Nanotechnology* **2010**, *21*, 485701.
(19) Tran, N. T. T.; Nguyen, D. K.; Glukhova, O. E.; Lin, M.-F. Coverage-Dependent Essential Properties of Halogenated Graphene: A DFT Study. *Sci. Rep.* **2017**, *7*, 17858.
(20) Zhou, J.; Wang, Q.; Sun, Q.; Chen, X.; Kawazoe, Y.; Jena, P. Ferromagnetism in Semihydrogenated Graphene Sheet. *Nano Lett.* **2009**, *9*, 3867−3870.
(21) Luo, Z.; Yu, T.; Kim, K.-j.; Ni, Z.; You, Y.; Lim, S.; Shen, Z.; Wang, S.; Lin, J. Thickness-Dependent Reversible Hydrogenation of Graphene Layers. *ACS Nano* **2009**, *3*, 1781−1788.
(22) Li, L.; Qin, R.; Li, H.; Yu, L.; Liu, Q.; Luo, G.; Gao, Z.; Lu, J. Functionalized Graphene for High-Performance Two-Dimensional Spintronics Devices. *ACS Nano* **2011**, *5*, 2601−2610.
(23) Gao, H.; Wang, L.; Zhao, J.; Ding, F.; Lu, J. Band Gap Tuning of Hydrogenated Graphene: H Coverage and Configuration Dependence. *J. Phys. Chem. C* **2011**, *115*, 3236−3242.
(24) Yi, D.; Yang, L.; Xie, S.; Saxena, A. Stability of Hydrogenated Graphene: a First-Principles Study. *RSC Adv.* **2015**, *5*, 20617−20622.
(25) Marsusi, F.; Drummond, N. D.; Verstraete, M. The Physics of Single-side Fluorination of Graphene: DFT and DFT+U studies. *Carbon* **2019**, *144*, 615−627.
(26) Nair, R. R.; Ren, W.; Jalil, R.; Riaz, I.; Kravets, V. G.; Britnell, L.; Blake, P.; Schedin, F.; Mayorov, A. S.; Yuan, S.; Katsnelson, M. I.; Cheng, H.-M.; Strupinski, W.; Bulusheva, L. G.; Okotrub, A. V.; Grigorieva, I. V.; Grigorenko, A. N.; Novoselov, K. S.; Geim, A. K. Fluorographene: a Two-Dimensional Counterpart of Teflon. *Small* **2010**, *6*, 2877−2884.
(27) Kresse, G.; Hafner, J. Norm-Conserving and Ultrasoft Pseudopotentials for First-Row and Transition Elements. *J. Phys.: Condens. Matter* **1994**, *6*, 8245.
(28) Blöchl, P. E. Projector Augmented-Wave Method. *Phys. Rev. B: Condens. Matter Mater. Phys.* **1994**, *50*, 17953.
(29) Kresse, G.; Joubert, D. From Ultrasoft Pseudopotentials to the Projector Augmented-Wave Method. *Phys. Rev. B: Condens. Matter Mater. Phys.* **1999**, *59*, 1758.
(30) Perdew, J. P.; Burke, K.; Ernzerhof, M. Generalized Gradient Approximation Made Simple. *Phys. Rev. Lett.* **1996**, *77*, 3865.
(31) Heyd, J.; Scuseria, G. E.; Ernzerhof, M. Hybrid Functionals Based on a Screened Coulomb Potential. *J. Chem. Phys.* **2003**, *118*, 8207−8215.
(32) Paier, J.; Marsman, M.; Hummer, K.; Kresse, G.; Gerber, I. C.; Ángyán, J. G. Screened Hybrid Density Functionals Applied to Solids. *J. Chem. Phys.* **2006**, *124*, 154709.
(33) Nosé, S. A Unified Formulation of the Constant Temperature Molecular Dynamics methods. *J. Chem. Phys.* **1984**, *81*, 511−519.
(34) Nosé, S. A Molecular Dynamics Method for Simulations in the Canonical Ensemble. *Mol. Phys.* **1984**, *52*, 255−268.
(35) Hoover, W. G. Canonical Dynamics: Equilibrium Phase-Space Distributions. *Phys. Rev. A: At., Mol., Opt. Phys.* **1985**, *31*, 1695.
(36) Chaput, L.; Togo, A.; Tanaka, I.; Hug, G. Phonon-Phonon Interactions in Transition Metals. *Phys. Rev. B: Condens. Matter Mater. Phys.* **2011**, *84*, 094302.
(37) Henkelman, G.; Uberuaga, B. P.; Jónsson, H. A Climbing Image Nudged Elastic Band Method for Finding Saddle Points and Minimum Energy Paths. *J. Chem. Phys.* **2000**, *113*, 9901−9904.
(38) Silvi, B.; Savin, A. Classification of Chemical Bonds Based on Topological analysis of Electron Localization Functions. *Nature* **1994**, *371*, 683.
(39) Coleman, J. N.; Lotya, M.; O'Neill, A.; Bergin, S. D.; King, P. J.; Khan, U.; Young, K.; Gaucher, A.; De, S.; Smith, R. J.; Shvets, I. V.; Arora, S. K.; Stanton, G.; Kim, H.-Y.; Lee, K.; Kim, G. T.; Duesberg, G. S.; Hallam, T.; Boland, J. J.; Wang, J. J.; Donegan, J. F.; Grunlan, J. C.; Moriarty, G.; Shmeliov, A.; Nicholls, R. J.; Perkins, J. M.; Grieveson, E. M.; Theuwissen, K.; McComb, D. W.; Nellist, P. D.; Nicolosi, V.; et al. Two-dimensional nanosheets produced by liquid exfoliation of layered materials. *Science* **2011**, *331*, 568−571.
(40) Chen, X.; Dobson, J. F.; Raston, C. L. Vortex fluidic exfoliation of graphite and boron nitride. *Chem. Commun.* **2012**, *48*, 3703−3705.
(41) Lukowski, M. A.; Daniel, A. S.; Meng, F.; Forticaux, A.; Li, L.; Jin, S. Enhanced Hydrogen Evolution Catalysis from Chemically Exfoliated Metallic MoS2 Nanosheets. *J. Am. Chem. Soc.* **2013**, *135*, 10274−10277.
(42) Li, G.; Li, Y.; Liu, H.; Guo, Y.; Li, Y.; Zhu, D. Architecture of Graphdiyne Nanoscale Films. *Chem. Commun.* **2010**, *46*, 3256−3258.
(43) Kara, A.; Enriquez, H.; Seitsonen, A. P.; Voon, L. L. Y.; Vizzini, S.; Aufray, B.; Oughaddou, H. A review on silicene—new candidate for electronics. *Surf. Sci. Rep.* **2012**, *67*, 1−18.
(44) Tusche, C.; Meyerheim, H.; Kirschner, J. Observation of depolarized ZnO (0001) monolayers: formation of unreconstructed planar sheets. *Phys. Rev. Lett.* **2007**, *99*, 026102.
(45) Singh, A. K.; Mathew, K.; Zhuang, H. L.; Hennig, R. G. Computational Screening of 2D Materials for Photocatalysis. *J. Phys. Chem. Lett.* **2015**, *6*, 1087−1098.
(46) Bartell, L. S. On the Length of the Carbon-carbon Single Bond. *J. Am. Chem. Soc.* **1959**, *81*, 3497−3498.
(47) Born, M.; Huang, K. *Dynamical Theory of Crystal Lattices*; Oxford, 1954.
(48) Li, X.; Zhang, S.; Wang, F. Q.; Guo, Y.; Liu, J.; Wang, Q. Tuning the Electronic and Mechanical Properties of Penta-graphene via Hydrogenation and Fluorination. *Phys. Chem. Chem. Phys.* **2016**, *18*, 14191−14197.
(49) Karlický, F.; Zbořil, R.; Otyepka, M. Band Gaps and Structural Properties of Graphene Halides and their Derivates: A Hybrid


https://dx.doi.org/10.1021/acs.jpcc.9b12022
J. Phys. Chem. C 2020, 124, 8225−8235

Functional Study with Localized Orbital Basis Sets. *J. Chem. Phys.* **2012**, *137*, 034709.
(50) Zbořil, R.; Karlickỳ, F.; Bourlinos, A. B.; Steriotis, T. A.; Stubos, A. K.; Georgakilas, V.; Šafářová, K.; Jančík, D.; Trapalis, C.; Otyepka, M. Graphene Fluoride: A stable Stoichiometric Graphene Derivative and its Chemical Conversion to graphene. *Small* **2010**, *6*, 2885−2891.
(51) Li, B.; Zhou, L.; Wu, D.; Peng, H.; Yan, K.; Zhou, Y.; Liu, Z. Photochemical Chlorination of Graphene. *ACS Nano* **2011**, *5*, 5957−5961.
(52) Gopalakrishnan, K.; Subrahmanyam, K.; Kumar, P.; Govindaraj, A.; Rao, C. Reversible Chemical Storage of Halogens in Few-Layer Graphene. *RSC Adv.* **2012**, *2*, 1605−1608.



https://dx.doi.org/10.1021/acs.jpcc.9b12022
*J. Phys. Chem. C* 2020, 124, 8225−8235